ACS OMEGA

http://pubs.acs.org/journal/acsodf

Article

Preparation of Activated Boron Nitride and Its Adsorption Characteristics for Zn, Cu, and Cd in Flue Gas

Anjun Gai, Yanlong Li,* Fengqi Zhan, Junzhong Zhang, and Rundong Li

Cite This: *ACS Omega* 2023, 8, 27612−27620

Read Online

ACCESS | Metrics & More | Article Recommendations | Supporting Information

ABSTRACT: Developing non-carbon-based adsorbents is essential for removing heavy metals from post-incineration flue gas. In this study, a new high-temperature-resistant adsorbent-activated boron nitride (BN) was prepared using precursors combined with a high-temperature activation method. The adsorption characteristics of BN for Zn, Cu, and Cd in simulated flue gas and sludge incineration flue gas were investigated using gas-phase heavy metal adsorption experiments. The results showed that BN prepared at 1350 °C for 4 h had defect structures, abundant pores, functional groups, and a high specific surface area of 658 m^2/g. The adsorption capacity of BN in simulated flue gases decreases with increasing adsorption temperature, whereas it is always higher than that of activated carbon (AC). The total adsorption capacities for Zn, Cu, and Cd were the highest at 50 °C with 48.3 mg/g. BN had strong adsorption selectivity for Zn, with a maximum adsorption capacity of 54.45 mg/g, and its adsorption process occurred mainly on the surface. Cu and Cd inhibited Zn adsorption, leading to a decrease in the Zn adsorption capacity. In sludge incineration flue gas, BN can quickly reach adsorption equilibrium. The BN had a synergistic disposal capacity for heavy metals and fine particulate matter. The maximum adsorption capacity was reduced compared to the simulated flue gas adsorption capacity, which was 5.1 mg/g. However, BN still exhibited a strong adsorption selectivity for Zn, and its adsorption capacity was always greater than that of AC. The rich functional groups and high specific surface area enable BN to physically and chemically double-adsorb heavy metals.

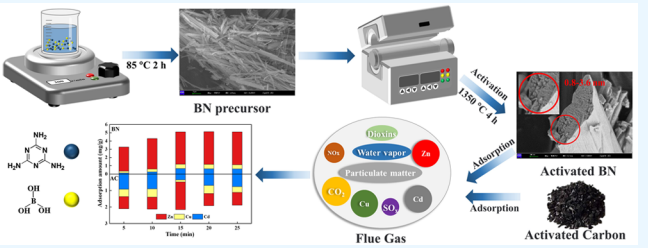

1. INTRODUCTION

With the development of the national economy and the promotion of urbanization, the urban sewage discharge system and treatment facilities have continuously improved, and sludge production has increased annually. According to statistics from 2021, the production of wet sludge (80% water content) in China is about 71.15 million tonnes.[1−4] Sludge treatment and disposal technologies widely used in China include sanitary landfills, land use, composting, and incineration.[5−8] Sludge incineration has become a more commonly accepted solid waste treatment method worldwide because of its ability to achieve sludge reduction quickly and its harmlessness and resourcefulness, and the rate of sludge incineration treatment has increased from 21 to 38% in recent years.[9−11] Heavy metals in dry sludge account for 0.5−4% of the total dry weight and are easily enriched in fly ash particles or escape directly into the gaseous state during high-temperature incineration, causing pollution and environmental damage.[12−16] Therefore, heavy metals in the flue gas are usually removed by pre-treatment before combustion, controlled during combustion, and removed by adsorption after combustion. Among these, post-combustion heavy metal adsorption control technology is currently a research hotspot. Researchers have focused on developing activated carbon (AC), kaolin, mineral oxides, and other non-carbon-based adsorbents.[17−19] AC is widely used because of its rich surface functional groups and pore structure. However, it exhibits low adsorption efficiency at high temperatures, limited regeneration, poor fly ash reusability, and high operating costs.[17] Therefore, developing new high-temperature-resistant and efficient non-carbon-based adsorbents is significant for developing heavy metal adsorption control technologies after combustion.

Boron nitride (BN) has good thermal stability, oxidation resistance, chemical inertness, high specific surface area, large surface functional groups, a graphene-like structure, and B−N polar bonds. As a result, BN has a better adsorption capacity than carbon-based adsorbents.[20,21] Li et al. prepared reactive boron nitride using a simple structural modulation method with a surface area of up to 2100 m^2/g and maximum adsorption amounts of 215, 225, 235, and 282 mg/g for Co^{2+}, Pb^{2+}, Ni^{2+}, and Ce^{3+}, respectively.[22] Liu et al. synthesized BN fibers using a Lucerne sponge as a template and a carbon thermal reduction method, which showed significant adsorp-

Received: May 14, 2023
Accepted: June 28, 2023
Published: July 22, 2023

tion performance for Pb^{2+}, Cr^{3+}, Zn^{2+}, and Cd^{2+} with maximum absorption capacities of 453, 723, 1885, and 2989 mg/g, respectively, with Cd^{2+} and Zn^{2+} breaking the reported maximum.[23] Wang et al. observed that BN could rapidly adsorb heavy metals and achieve adsorption equilibrium for Cu^{2+} and Pb^{2+} within a short period.[24] Other studies have shown that BN has a selective adsorption capacity for heavy metals. Different preparation methods result in different selective adsorption capacities for BN.[25−27] Wang et al. conducted adsorption experiments in a quaternary system and observed that the adsorption capacity of BN reached 845 mg/g for Pb^{2+} with significant selectivity and 312, 402, and 201 mg/g for Cd^{2+}, Cu^{2+}, and Ni^{2+}, respectively.[28] Azamat et al. investigated the mechanism of heavy metal adsorption from wastewater by BN nanotubes using molecular dynamics methods and showed that BN nanotubes selectively adsorb Zn^{2+}.[29] BN has received significant attention as an efficient adsorption material.[30−34] However, research has primarily focused on wastewater treatment, and few studies have reported its gas-phase heavy metal adsorption capacity.

Therefore, a high-temperature-resistant and highly efficient BN adsorbent was developed in this study using precursors combined with a high-temperature activation method. The BN microscopic morphology was regulated by changing the activation time and temperature. The adsorption characteristics of BN for the heavy metals Zn, Cu, and Cd under simulated flue gas and sludge incineration flue gas were investigated using a self-designed gas-phase heavy metal adsorption experimental rig. Activated carbon was established as the control group to analyze the mechanisms influencing the adsorption capacity of the BN.

2. MATERIALS AND METHODS

2.1. Materials. Melamine ($C_3H_6N_6$), boric acid (H_3BO_3), zinc chloride ($ZnCl_2$), and other chemicals were purchased from Sinopharm Reagent Co., Ltd. (China). All the chemical reagents used in this study were analytically pure. The raw sludge (79% water content) was obtained from a city wastewater treatment plant in Dalian, Liaoning Province (China), and its heavy metal content is shown in Table 1. The raw sludge was dried, ground, sieved (150 μm), and prepared for use.

Table 1. Heavy Metal Content of Raw Sludge (mg/g)

As	Cd	Cr	Cu	Ni	Zn
0.0111	0.0027	0.1243	4.3928	0.0604	0.6867

2.2. Preparation of Active Boron Nitride Adsorbent. In this study, a combination of precursors and high-temperature activation was used to prepare BN. Boric acid and melamine in a molar ratio of 2:1 were added to 1000 mL of deionized water, placed in a magnetic agitator, stirred for 2 h at 300 rpm and 85 °C, then cooled, filtered, washed with water, and dried at 90 °C for 24 h to obtain the BN precursor. The precursor was placed in a tubular atmosphere furnace (GSL-1700X, Kejing, Shenyang, China) under a nitrogen atmosphere and activated at 1350 °C for 4 h to obtain the BN adsorbent for backup.

2.3. Simulated (Sludge) Flue Gas Heavy Metal (Zn, Cu, and Cd) Adsorption Experiments. This study utilized a self-designed gas-phase heavy metal adsorption experimental rig, as shown in Figure 1. The simulated flue gas was provided

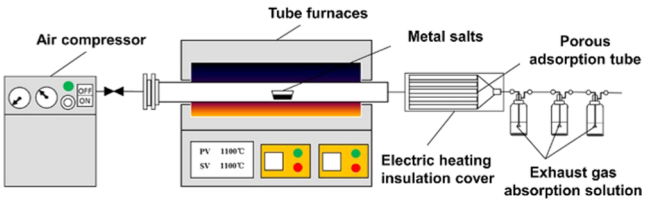

Figure 1. Gas-phase heavy metal adsorption test bench.

as a gas-phase heavy metal source via the thermal volatilization of zinc chloride, copper chloride, and cadmium chloride (3 g each). A corundum crucible containing the metal chloride salt (sludge) was placed in the heating zone of a horizontal tube furnace, and the temperature was set at 1000 °C to ensure that the experimental sample could be fully volatilized (burned). The air compressor provided a stable atmosphere, and the outlet was connected to an adsorption unit and a tail gas treatment unit. The simulated flue gas flow rate was 300 mL/min, the adsorbent mass was 0.1 g, and the tail gas absorption solution was a dilute acid. At the end of the experiment, the adsorbent was removed, cooled, and placed outside.

2.4. Analyses Methods. Scanning electron microscopy (SEM, Zeiss Gemini 300) and high-resolution field-emission transmission electron microscopy (TEM, Thermo Fisher F20) were used for microscopic morphological and structural analyses. The specific surface area and pore size distribution of the BN were analyzed using a fully automated physisorption instrument for the specific surface area (BET, Mac ASAP 2460) and X-ray diffraction (XRD, RIKEN Smart Lab-SE, Japan) to analyze the crystallinity and diffraction angle. The heavy metal content was determined using a microwave digestion instrument (Shanghai Xinyi, MDS-15) using the triple acid combination (HNO_3−HF−$HClO_4$) method for the adsorbent and sludge ash digestion. An inductively coupled plasma emission spectrometer (ICP-OES, Platinum Elmer Optima-ICP8300) was used to determine the heavy metal adsorption.

3. RESULTS AND DISCUSSION

3.1. Selection of Preparation Conditions of BN. The specific surface area size is an important factor affecting the physical adsorption of adsorbents.[35] The experiments investigated the effect of activation time (3, 4, and 5 h) and activation temperature (1300−1600 °C) on the specific surface area of BN, as shown in Figure 2. The results showed that

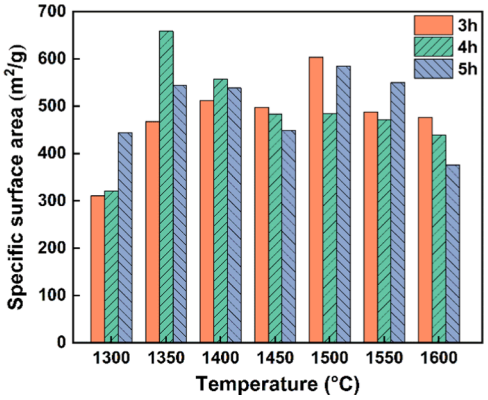

Figure 2. Specific surface area of BN under different preparation conditions.

https://doi.org/10.1021/acsomega.3c03348
ACS Omega 2023, 8, 27612−27620

when the activation time was short or the temperature was low, the precursor was not completely pyrolyzed, the residual impurities were not completely volatilized, and the pores were blocked, so the specific surface area of BN was low. When the activation time was long or the temperature was high, the micropores shrank and part of the pore structure was destroyed, decreasing the specific surface area. The analysis of orthogonal experiments revealed that the maximum specific surface area of BN was 658.58 m^2/g when the activation temperature was 1350 °C and the activation time was 4 h, 54.6 times higher than that of ordinary BN. All subsequent studies used the BN prepared under these conditions as the adsorbent.

3.2. BN Characterization Analysis. *3.2.1. Analysis of BN Pore Structure.* The N_2 adsorption−desorption isotherm of BN is shown in Figure 3. The isotherms are distinct type-I

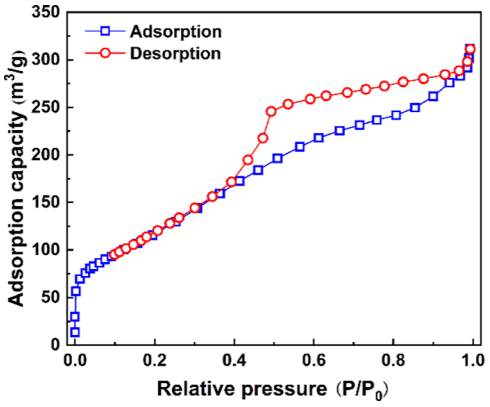

Figure 3. N_2 adsorption−desorption isotherm of BN.

isotherms with H4 hysteresis lines, indicating the presence of micropores and narrow-slit mesopores. The pore volume was about 0.59 cm^3/g, and the characteristic pore sizes were 0.88, 2.2, and 3.61 nm, with an average pore size of about 2.9 nm. BN has a higher surface area and a suitable pore size distribution, which provide more activated adsorption sites and improve the trapping capacity of BN for heavy metals in the gas phase.[36]

3.2.2. Physical Phase Analysis of BN. The X-ray diffraction pattern of BN is shown in Figure 4. The characteristic peak at 2θ = 25.46° is the (002) plane, and the characteristic peak at 2θ = 42.4° is the (100) plane. The diffraction peak had a

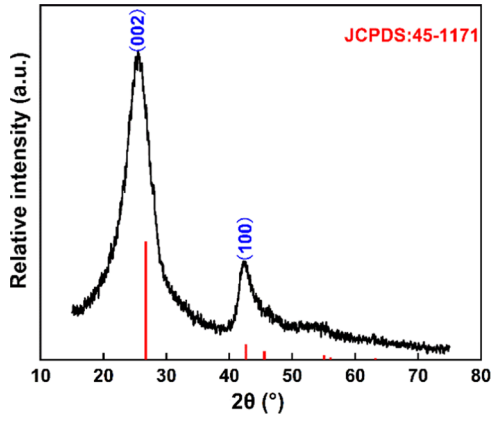

Figure 4. XRD analysis diagram of BN.

higher degree of a coincidence than the standard picture card. The prepared BN was a hexagonal BN material.

$$2d \sin\theta = n\lambda \quad (1)$$

where θ is the angle between the incident ray and sample, d is the crystal plane distance, λ is the wavelength of the incident light, and n is the diffraction level.

The calculated d = 0.349 nm indicates that the BN prepared using this method was less crystalline and had various defects on the surface and inside, and the defective structure provided more activated sites to promote adsorption.[20]

3.2.3. Analysis of BN Morphology. The SEM and TEM analysis plots of the BN are shown in Figure 5. After high-temperature activation, the BN exhibited an independent rod-like fiber structure with a relatively uniform size and pore size distribution. The length was approximately 10 to 50 μm, and the diameter was approx. 0.5 to 3 μm. The surface of BN has many pore structures with a uniform distribution. The TEM test results show that the BN had a rod-like structure filled with pores. As shown in Figure 5d, the crystallographic arrangement is hexagonal; however, there are more regions of low crystallinity. After measurement and calculation, the layer spacing was determined to be at approx. 0.34 nm, slightly larger than the theoretical value of the BN crystal plane distance (0.33 nm). This result is consistent with the XRD results.

3.2.4. XPS Analysis of BN. The chemical bonding of the BN surface was analyzed using an X-ray photoelectron spectroscopy analyzer, as shown in Figure 6. From Figure 6a, BN contained binding energy peaks for B 1s (190.57 eV), N 1s (398.93 eV), C 1s (284.97 eV), and O 1s (532.38 eV).[37] Figure 6b shows a fine map of B 1s, and the results show that the B 1s map contained B−N bonds (190.76 eV) and B−O bonds (192.87 eV), with the B atom forming a B−O bond with the O atom that was favorable for adsorption.[38] Figure 6c shows the N 1s fine spectrum with binding energy peaks at 398.34 and 398.69 eV, corresponding to polar B−N and $-NH_2$ bonds, respectively, with the polar B−N bond being much higher than the $-NH_2$ bond. The abundance of surface functional groups and chemical bonds may be the key to the efficient adsorption capacity of BN.

3.3. Adsorption Properties of Active BN for Zn, Cu, and Cd. Figure 7 shows the total adsorption capacities of BN and AC for heavy metals Zn, Cu, and Cd in simulated flue gas at 50−250 °C. The results show that the total adsorption capacity of both adsorbents for mixed heavy metals decreased with increasing temperature. The maximum adsorption capacities were 48.3 and 34.9 mg/g at an adsorption temperature of 50 °C, which were 2.8 and 7.4 times the adsorption capacities at 250 °C, respectively. During the adsorption of gas-phase heavy metals, the kinetic energy of the molecules was converted to thermal energy, which is generally an exothermic process. Thus, an increase in the temperature leads to a decrease in adsorption.[39,40] The total adsorption capacity of BN for the heavy metals Zn, Cu, and Cd in the simulated flue gas was greater than that of AC. This phenomenon became more significant with an increase in temperature. This was due to the gradual inactivation of the AC with increasing temperatures.[17] When the temperature was higher than 150 °C, the deactivation phenomenon was more significant, and the adsorption capacity for heavy metals was significantly reduced. Table 2 compares the adsorption capacity of different adsorbents for heavy metals in the gas

https://doi.org/10.1021/acsomega.3c03348
ACS Omega 2023, 8, 27612−27620

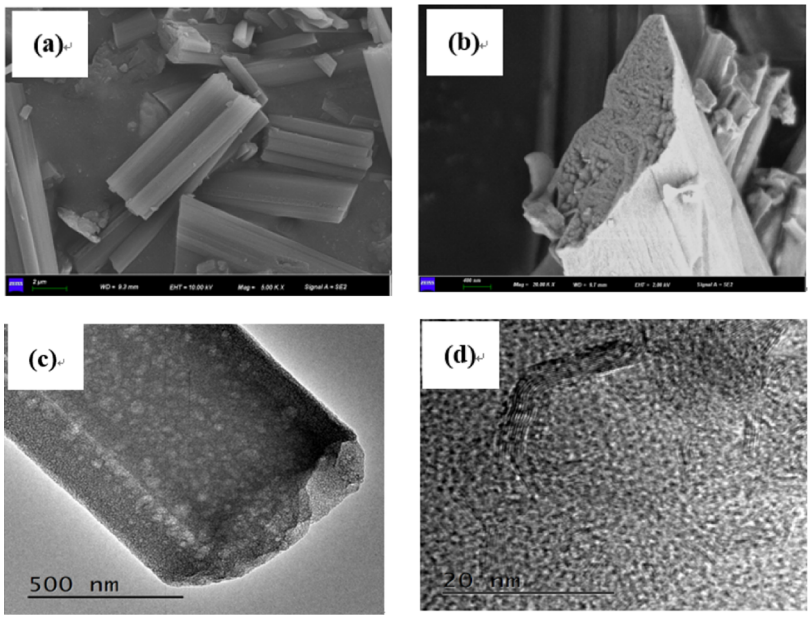

Figure 5. SEM (a, b) and TEM (c, d) diagrams of the BN.

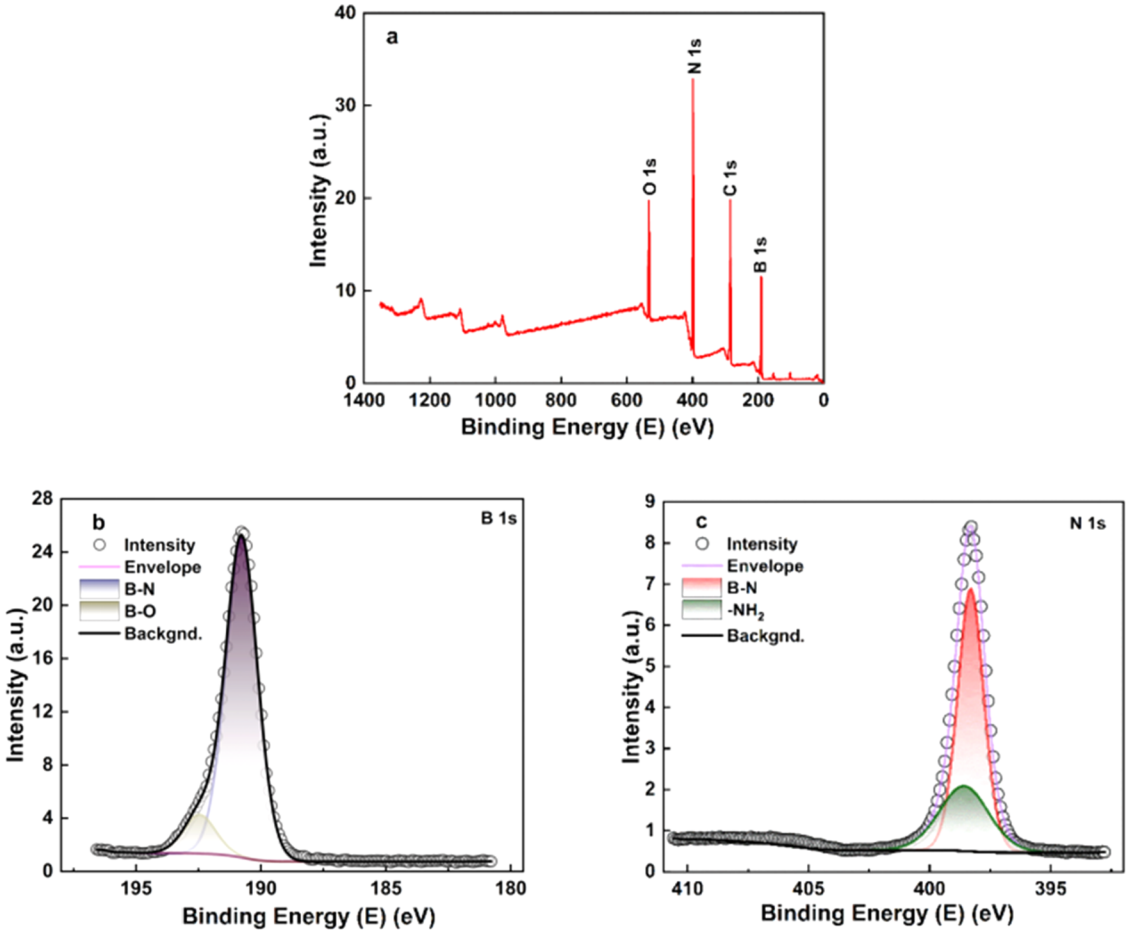

Figure 6. Plots of the total XPS spectrum (a), B1s fine spectrum (b), and N1s fine spectrum (c) of BN.

phase. The results show that the BN adsorbent prepared in this study has a better adsorption capacity among the reported adsorbent materials.

Figure 8 shows the adsorption capacities of BN and AC for heavy metals Zn, Cu, and Cd in simulated flue gas at 50−250 °C. The results show that the adsorption patterns of the two adsorbents for the individual heavy metals were consistent with the total adsorption capacity pattern, which showed a decreasing trend with increasing adsorption temperature. The adsorption capacities of BN for heavy metals Zn, Cu, and Cd

https://doi.org/10.1021/acsomega.3c03348
ACS Omega 2023, 8, 27612−27620

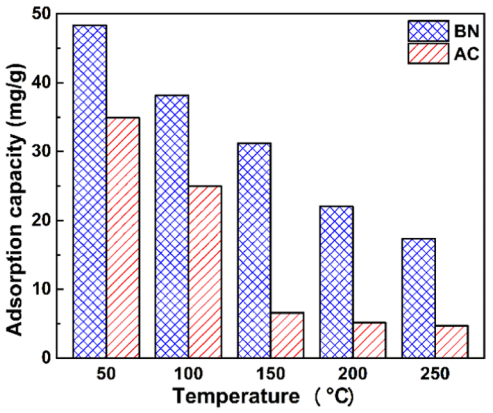

Figure 7. Effect of adsorption temperature on the total adsorption capacity of BN and AC.

Table 2. Adsorption Capacity of Different Adsorbents

adsorbent	adsorption capacity (mg/g)	
kaolin	33.0	41
silica−aluminum based	2.6	18
AC	17.5	42
AC	34.9	this article
BN	48.3	this article

were consistently higher than those of AC at 50−250 °C. The adsorption capacity of BN was the highest for Zn, reaching 28.74 mg/g, which was 4.3 and 2.3 times higher than the maximum adsorption capacities for Cu and Cd, respectively, reflecting the strong adsorption selectivity for the heavy metal Zn. The AC adsorption capacity for Cd is the highest at 50 °C, reaching 15.21 mg/g, which is 2 times and 1.2 times the maximum adsorption capacities of Cu and Zn, respectively. In contrast, the adsorption capacity of Zn was higher than that of Cd with increased adsorption temperature. This indicates that AC did not show strong adsorption selectivity and that the adsorption temperature had a more significant effect on the adsorption capacities of different heavy metals.

The above analysis shows that the heavy metals' adsorption capacity of BN is always greater than that of AC. This is due to the abundant polar B−N bonds, $-NH_2$ groups, and B−O bonds on the surface of BN may have chemical reactions with heavy metals. During adsorption the polar B−N bonds within BN are prone to break, forming B−OH bonds and $-NH_2$ groups, the B−OH bonds may form coordination bonds with heavy metals, which make heavy metals adsorbed in the form of oxides; the $-NH_2$ groups may complex with heavy metals, making BN have higher adsorption efficiency.[43,44]

3.4. Adsorption Performance and Mechanism of Active BN for Zn. BN has strong adsorption selectivity for the heavy metal Zn. This section experimentally investigates the variation in the adsorption capacity of BN and AC for the heavy metal Zn at 50−250 °C in simulated flue gas, as shown in Figure 9. The results show that the adsorption capacity of

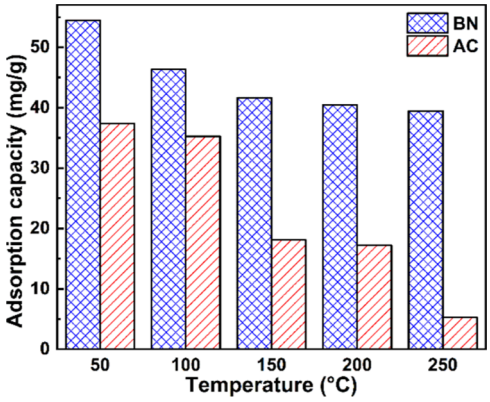

Figure 9. Effect of adsorption temperature on the adsorption of Zn by BN and AC.

BN for the heavy metal Zn was greater than that of AC, and the difference in adsorption capacity was more significant as the adsorption temperature increased. The adsorption capacity of BN at 250 °C was 7.5 times higher than that of AC.

The BN had a maximum adsorption capacity of 54.45 mg/g for the heavy metal Zn at 50 °C. The maximum adsorption capacity of AC was 37.38 mg/g. Both capacities are higher than the adsorption capacity of the simulated mixed heavy metal flue gas. This indicates that Zn, Cu, and Cd compete with each other in the gas-phase adsorption process, and Cu and Cd inhibit the adsorption of Zn by the BN.

To further characterize the Zn adsorption behavior of BN, SEM-energy-dispersive X-ray spectroscopy (SEM-EDS) was used to characterize before and after adsorption, as shown in Figure 10 and Table 3. The appearance of uniformly distributed micron-size clusters on the surface of the BN after the adsorption of Zn indicates that the heavy metal Zn was successfully adsorbed on the adsorbent surface. Energy spectrum analysis of the adsorbed substances on the surface of

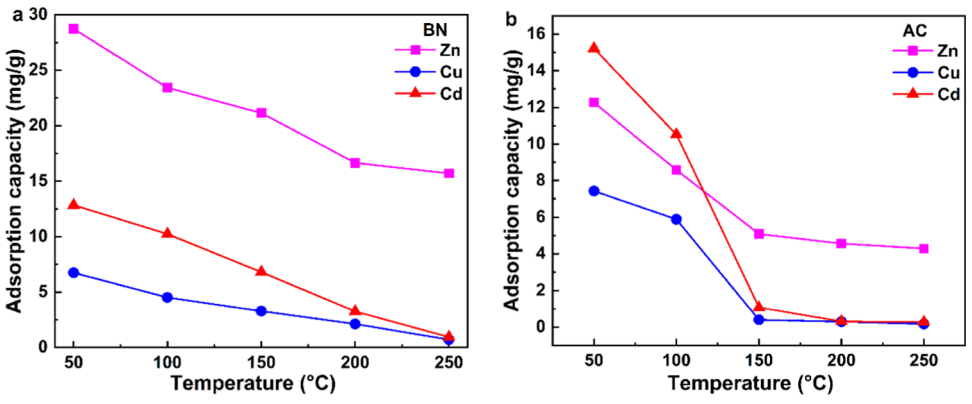

Figure 8. Effect of adsorption temperature on the adsorption of Zn, Cu, and Cd by BN (a) and AC (b).

https://doi.org/10.1021/acsomega.3c03348
ACS Omega 2023, 8, 27612−27620

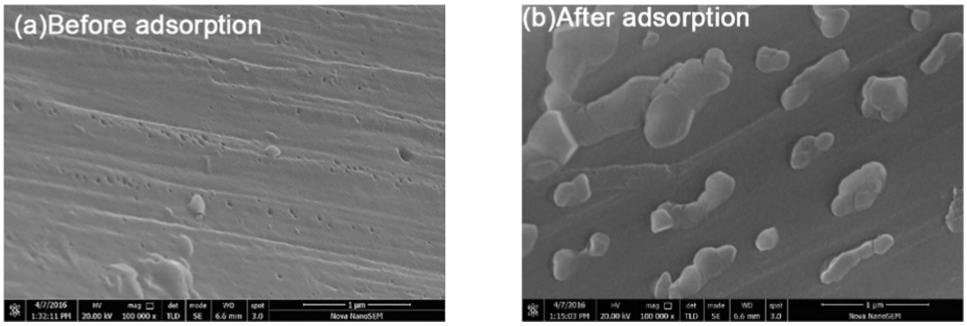

Figure 10. SEM comparison before (a) and after (b) adsorption of BN.

Table 3. Elemental Content on the Surface of BN Adsorbent (Weight Percentage)

B	N	Zn	C	O
32.65	30.85	19.69	12.25	4.56

BN using EDS showed that the adsorbent surface mainly contained B and N and adsorbed Zn, of which the weight percentage of Zn was approx. 19.69%. The energy spectrum analysis showed that the adsorption of Zn by BN was higher than the ICP-OES test results. This is because Zn forms agglomerate on the surface, and the agglomerate size is generally in the micron range, which is larger than the average pore size of BN, resulting in the occurrence of the main adsorption behavior on the BN surface.

3.5. Adsorption Characteristics of BN for Zn, Cu, and Cd in Sludge Incineration Flue Gas. To investigate the high-temperature adsorption characteristics of heavy metals in sludge flue gas by BN, adsorption experiments were carried out on sludge combustion flue gas at 1000 °C. The adsorption temperature was 250 °C, the adsorption time was 5−25 min, and AC was set as the control group. As shown in Figure 11,

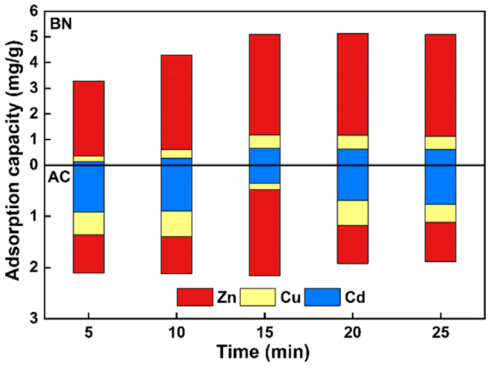

Figure 11. Adsorption of Zn, Cu, and Cd in sludge flue gas.

the adsorption of 0−15 min active BN increased gradually and reached equilibrium at 15 min, with a maximum adsorption capacity of 5.1 mg/g. The maximum adsorption capacities for Zn, Cu, and Cd are 3.92, 0.52, and 0.66 mg/g, respectively. BN exhibited a high adsorption selectivity for Zn in sludge flue gas, and the adsorption capacity of Zn was 7.5 times higher than that of Cu. With an increase in adsorption time, the adsorption capacity maintained dynamic equilibrium, desorption at high temperatures did not occur easily, and the adsorption was stable. The adsorption capacity of BN for sludge flue gas was always higher than that of AC. With an increase in adsorption time, the deactivation of AC intensified, and the overall fluctuation of AC adsorption capacity was small; the maximum adsorption capacity was only 2.2 mg/g and did not show significant adsorption selectivity. The analysis revealed that, in addition to gaseous heavy metals in the gas phase, the sludge flue gas produced fine particulate matter, which had a competitive mechanism with heavy metals, resulting in a lower adsorption number of heavy metals than the simulated flue gas. This indicates that BN can synergistically dispose of heavy metals and fine particulate matter. In contrast, heavy metal pollution in practical applications is closely related to fine particulate matter,[45,46] broadening the direction for new non-carbon-based adsorbent-BN applications.

The adsorption process of Zn in sludge flue gas by BN was analyzed using the quasi-primary kinetic model and the quasi-secondary kinetic model, as shown in Figure 12. The results

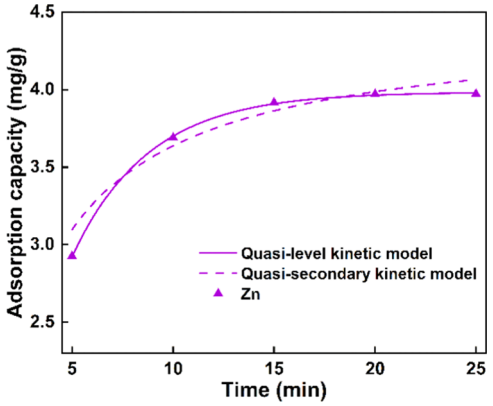

Figure 12. Kinetic analysis of Zn, Cu, and Cd adsorption by BN.

show that the quasi-primary kinetic model better describes the adsorption process of BN on Zn. The correlation coefficients of the quasi-primary and quasi-secondary kinetic models were not significantly different. Therefore, the adsorption of Zn in sludge flue gas by BN can be considered as a combined effect of physical and chemical adsorption.

To further analyze the limiting steps in the process of BN adsorption of Zn, a diffusion model in the particle is used to perform a kinetic analysis of the adsorption process, as shown in Figure 13. The results indicate that the adsorption process of Zn by BN can be divided into three stages. The first stage is a fast adsorption stage with k1 of 0.826. The electrostatic adsorption effect allows Zn to adsorb rapidly on the BN surface. The second stage is the intraparticle diffusion stage, with a gradual decrease in slope indicating an increase in the diffusion resistance for BN to adsorb Zn, and Zn gradually

https://doi.org/10.1021/acsomega.3c03348
ACS Omega 2023, 8, 27612−27620

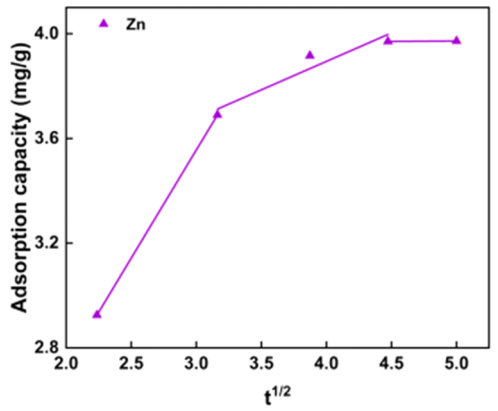

Figure 13. Fitting analysis of intraparticle diffusion of BN adsorbed Zn.

diffuses toward the internal adsorption sites. In the third stage, the adsorption of BN on Zn reached saturation, and the fitted curve did not cross the origin, indicating that in addition to the influence of intraparticle diffusion factors, it may also be influenced by other factors.

4. CONCLUSIONS

In this study, a BN adsorbent was prepared using precursors combined with a high-temperature activation method. The effects of the activation time and temperature on the microscopic morphology of BN were investigated, along with the adsorption characteristics of BN for Zn, Cu, and Cd in simulated flue gas and sludge incineration flue gas. The results show that the BN prepared at an activation temperature of 1350 °C and an activation time of 4 h has the maximum specific surface area (658 m^2/g). At this time, the BN has a typical intermediate pore structure with a pore volume of about 0.59 cm^3/g, an average pore diameter of about 2.9 nm, and a short rod-like fiber structure with a length of about 10−50 μm, a diameter of about 0.5−3 μm, and a surface pore in the abundant class. The BN prepared by this method has high purity without mixing other impurities, low crystallinity, and more defective structures. XPS analysis shows that BN surface contains abundant functional groups and chemical bonds.

The total adsorption capacity of BN in the simulated mixed heavy metal flue gas decreased with increasing temperature. The maximum adsorption capacity (48.3 mg/g) was obtained at 50 °C. The total adsorption capacity of BN was always greater than that of AC, and when the adsorption temperature was higher than 150 °C, AC showed deactivation, whereas BN did not. BN has strong adsorption selectivity for Zn, and its adsorption capacity is 4.3 times that of Cu and 2.3 times that of Cd. During the adsorption process, the abundant polar B−N bonds, $-NH_2$ groups, and B−O bonds on the BN surface have potential chemical reactions with heavy metals. The maximum adsorption capacity of BN for Zn in simulated Zn flue gas was 54.45 mg/g. There was a competitive mechanism among Zn, Cu, and Cd in the adsorption process, and Cu and Cd inhibited Zn adsorption. The adsorption of Zn by BN occurred mainly on the adsorbent surface.

In the sludge incineration flue gas, the adsorption rate of BN was high and reached adsorption equilibrium at 15 min, with a maximum adsorption capacity of 5.1 mg/g. The maximum amounts of Zn, Cu, and Cd were 3.92, 0.52, and 0.66 mg/g, respectively. The BN had a high adsorption selectivity for Zn in sludge incineration flue gas, and the adsorption capacity for Zn was 7.5 times higher than that for Cu. The adsorption of heavy metals by BN is the result of a combination of physical adsorption and chemical adsorption.

■ ASSOCIATED CONTENT

Data Availability Statement

The data sets used or analyzed during the current study are available from the corresponding author on reasonable request.

Supporting Information

The Supporting Information is available free of charge at https://pubs.acs.org/doi/10.1021/acsomega.3c03348.

Attached file data sets (2) (ZIP)

■ AUTHOR INFORMATION

Corresponding Author

Yanlong Li − *College of Energy and Environment, Liaoning Province Key Laboratory of Clean Energy, Shenyang Aerospace University, Shenyang, Liaoning 110136, China;* orcid.org/0000-0002-9857-6563; Email: liyanlong@sau.edu.cn

Authors

Anjun Gai − *College of Energy and Environment, Liaoning Province Key Laboratory of Clean Energy, Shenyang Aerospace University, Shenyang, Liaoning 110136, China*

Fengqi Zhan − *College of Energy and Environment, Liaoning Province Key Laboratory of Clean Energy, Shenyang Aerospace University, Shenyang, Liaoning 110136, China*

Junzhong Zhang − *College of Energy and Environment, Liaoning Province Key Laboratory of Clean Energy, Shenyang Aerospace University, Shenyang, Liaoning 110136, China*

Rundong Li − *College of Energy and Environment, Liaoning Province Key Laboratory of Clean Energy, Shenyang Aerospace University, Shenyang, Liaoning 110136, China;* orcid.org/0000-0002-8669-5397

Complete contact information is available at: https://pubs.acs.org/10.1021/acsomega.3c03348

Author Contributions

A.G., R.L., and Y.L. designed the main body of the article. A.G., F.Z., and J.Z. performed the experiments, tested, organized the database and wrote the first draft of the manuscript.

Notes

The authors declare no competing financial interest.

The authors declare that we have no financial and personal relationships with other people or organizations that can inappropriately influence our work, and there is no professional or other personal interest of any nature or kind in any product, service, and/or company that could be construed as influencing the position presented in, or the review of, the manuscript entitled.

■ ACKNOWLEDGMENTS

The authors gratefully acknowledge the support of the National Natural Science Foundation of China (No. U21A20142).

■ REFERENCES

(1) Sun, Y.; Chen, Z.; Wu, G.; Wu, Q.; Zhang, F.; Niu, Z.; Hu, H. Characteristics of water quality of municipal wastewater treatment

plants in China: implications for resources utilization and management. *J. Cleaner Prod.* **2016**, *131*, 1−9.
(2) Wang, T.; Shi, F.; Zhang, Q.; Qian, X.; Hashimoto, S. Exploring material stock efficiency of municipal water and sewage infrastructures in China. *J. Cleaner Prod.* **2018**, *181*, 498−507.
(3) Mohurd Chinese Statistical Yearbook of Urban and Rural Construction (In Chinese), 2021. https://www.mohurd.gov.cn/gongkai/fdzdgknr/sjfb/index.html.
(4) Chen, Z.; Hou, Y.; Liu, M.; Zhang, G.; Zhang, K.; Zhang, D.; Yang, L.; Kong, Y.; Du, X. Thermodynamic and economic analyses of sewage sludge resource utilization systems integrating Drying, Incineration, and power generation processes. *Appl. Energy* **2022**, *327*, No. 120093.
(5) Chen, H.; Yan, S.; Ye, Z.; Meng, H.; Zhu, Y. Utilization of urban sewage sludge: Chinese perspectives. *Environ. Sci. Pollut. Res.* **2012**, *19*, 1454−1463.
(6) Wang, W.; Luo, Y.; Qiao, W. Possible solutions for sludge dewatering in China. *Front. Environ. Sci. Eng. China* **2010**, *4*, 102−107.
(7) Lu, J.-Y.; Wang, X.; Liu, H.; Yu, H.; Li, W. Optimizing operation of municipal wastewater treatment plants in China: The remaining barriers and future implications. *Environ. Int.* **2019**, *129*, 273−278.
(8) Jiang, Y.; Zhuo, J.; Yang, Y.; Chen, H.; Zhang, C. Short-term effects of municipal sludge composting on soil greenhouse gas emissions. *China Environ. Sci.* **2018**, *38*, 3788−3794.
(9) Kuo, N. W.; Ma, H. W.; Yang, Y.; Hsiao, T. Y.; Huang, C. An investigation on the potential of metal recovery from the municipal waste incinerator in Taiwan. *J. Waste Manage.* **2007**, *27*, 1673−1679.
(10) Huber, F.; Blasenbauer, D.; Mallow, O.; Lederer, J.; Winter, F.; Fellner, J. Thermal co-treatment of combustible hazardous waste and waste incineration fly ash in a rotary kiln. *J. Waste Manage.* **2016**, *58*, 181−190.
(11) Soon, K. T.; Loretta, Y. L. Feasibility of alternative sewage sludge treatment methods from a lifecycle assessment (LCA) perspective. *J. Cleaner Prod.* **2020**, *247*, No. 119495.
(12) Han, J.; Xu, M.; Yao, H.; Furuuchi, M.; Sakano, T.; Kanchanapiya, P.; Kanaoka, C. Partition of Heavy and Alkali Metals during Sewage Sludge Incineration. *Energy Fuels* **2006**, *20*, 583−590.
(13) Guo, F.; Zhong, Z. Pollution emission and heavy metal speciation from co-combustion of sedum plumbizincicola and sludge in fluidized bed. *J. Cleaner Prod.* **2018**, *179*, 317−324.
(14) Gondek, K.; Mierzwa-Hersztek, M.; Kopeć, M. Mobility of heavy metals in sandy soil after application of composts produced from maize straw, sewage sludge and biochar-Discussion of Moussavi et al. *J. Environ. Manage.* **2018**, *210*, 1−2.
(15) Fan, C.; Huang, Y.; Xia, Z.; Cha, J.; Yu, M.; Ding, Sh.; Hu, H.; Qi, E. Trapping of $CdCl_2$ and $PbCl_2$ vapor by modified kaolinite. *Chem. Eng. Prog.* **2020**, *39*, 1558−1566.
(16) Zhang, J.; Sun, G.; Liu, J.; Evrendilek, F.; Buyukada, M. Co-combustion of textile dyeing sludge with cattle manure: Assessment of thermal behavior, gaseous products, and ash characteristics. *J. Cleaner Prod.* **2020**, *253*, No. 119950.
(17) Ishag, A.; Yue, Y.; Xiao, J.; Huang, X.; Sun, Y. Recent advances on the adsorption and oxidation of mercury from coal-fired flue gas: A review. *J. Cleaner Prod.* **2022**, *367*, No. 133111.
(18) Yu, S.; Zhang, C.; Yuan, C.; Ma, L.; Fang, Q.; Chen, G. Study on the adsorption characteristics of mineral oxides on arsenic/lead in coal combustion flue gas. *J. Fuel Chem. Technol.* **2020**, *48*, 1345−1355.
(19) Xia, W.; Huang, Y.; Wang, X.; Cha, J.; Yang, Z.; Wang, J.; Xu, L. High-temperature capture of lead chloride vapor by non-carbon-based adsorbents. *Chem. Eng. Prog.* **2017**, *36*, 3508−3513.
(20) Han, F.; Zong, Y.; Jassby, D.; Wang, J.; Tian, J. The interactions and adsorption mechanisms of ternary heavy metals on boron nitride. *Environ. Res.* **2020**, *183*, No. 109240.
(21) Xue, Y.; Dai, P.; Jiang, X.; Wang, X.; Zhang, C.; Tang, D.; Weng, Q.; Wang, X.; Pakdel, A.; Tang, C.; Bando, Y.; Golberg, D. Template-free synthesis of boron nitride foam-like porous monoliths and their high-end applications in water purification. *J. Mater. Chem. A* **2016**, *4*, 1469−1478.
(22) Li, J.; Xiao, X.; Xu, X.; Lin, J.; Huang, Y.; Xue, Y.; Jin, P.; Zou, J.; Tang, C. Activated boron nitride as an effective adsorbent for metal ions and organic pollutants. *Sci. Rep.* **2013**, *3*, No. 3208.
(23) Li, S.; Liu, F.; Su, Y.; Shao, N.; Yu, D.; Liu, Y.; Liu, W.; Zhang, Z. Luffa sponge-derived hierarchical meso/macroporous boron nitride fibers as superior sorbents for heavy metal sequestration. *J. Hazard. Mater.* **2019**, *378*, No. 120669.
(24) Wang, H.; Wang, W.; Wang, H.; Zhang, F.; Li, Y.; Fu, Z. Urchin-like boron nitride hierarchical structure assembled by nanotubes-nanosheets for effective removal of heavy metal ions. *Ceram. Int.* **2018**, *44*, 12216−12224.
(25) khan, F.; A, N.; Din, I. U.; Saeed, T.; Alotaibi, M. A.; Alharthi, A. I.; Habib, A.; Malik, T. Synthesis, characterization and adsorption studies of h-BN crystal for efficient removal of Cd^{2+} from aqueous solution. *Ceram. Int.* **2021**, *47*, 4749−4757.
(26) Peng, D.; Jiang, W.; Li, F.; Zhang, L.; Liang, R.; Qiu, J. One-Pot Synthesis of Boron Carbon Nitride Nanosheets for Facile and Efficient Heavy Metal Ions Removal. *ACS Sustainable Chem. Eng.* **2018**, *6*, 11685−11694.
(27) Zhang, Y.; Wang, G.; Wang, S.; Wang, J.; Qiu, J. Boron-nitride-carbon nanosheets with different pore structure and surface properties for capacitive deionization. *J. Colloid Interface Sci.* **2019**, *552*, 604−612.
(28) Wang, N.; Xu, X.; Li, H.; Zhai, J.; Yuan, L.; Zhang, K.; Yu, H. Preparation and Application of a Xanthate-Modified Thiourea Chitosan Sponge for the Removal of Pb(II) from Aqueous Solutions. *Ind. Eng. Chem. Res.* **2016**, *55*, 4960−4968.
(29) Azamat, J.; Khataee, A.; Joo, S. W. Separation of a heavy metal from water through a membrane containing boron nitride nanotubes: molecular dynamics simulations. *J. Mol. Model.* **2014**, *20*, No. 2468.
(30) Guo, Y.; Yan, C.; Wang, P.; Lei, R.; Wang, C. Doping of carbon into boron nitride to get the increased adsorption ability for tetracycline from water by changing the pH of solution. *Chem. Eng. J.* **2020**, *387*, No. 124136.
(31) Song, Q.; Liang, J.; Fang, Y.; Guo, Z.; Du, Z.; Zhang, L.; Liu, Z.; Huang, Y.; Lin, J.; Tang, C. Nickel (II) modified porous boron nitride: An effective adsorbent for tetracycline removal from aqueous solution. *Chem. Eng. J.* **2020**, *394*, No. 124985.
(32) Wang, S.; Jia, F.; Kumar, P.; Zhou, A.; Hu, L.; Shao, X.; Wang, X.; Sun, Y.; Yin, G.; Liu, B. Hierarchical porous boron nitride nanosheets with versatile adsorption for water treatment. *Colloids Surf., A* **2020**, *598*, No. 124865.
(33) Wang, G.; Zhang, Y.; Wang, S.; Wang, Y.; Song, H.; Lv, S.; Li, C. Adsorption performance and mechanism of antibiotics from aqueous solutions on porous boron nitride-carbon nanosheets. *Environ. Sci.: Water Res. Technol.* **2020**, *6*, 1568−1575.
(34) Guo, Y.; Wang, R.; Wang, P.; Rao, L.; Wang, C. Developing a Novel Layered Boron Nitride-Carbon Nitride Composite with High Efficiency and Selectivity To Remove Protonated Dyes from Water. *ACS Sustainable Chem. Eng.* **2019**, *7*, 5727−5741.
(35) Dou, S.; Ke, X.; Shao, Z.; Zhong, L.; Zhao, Q.; Zheng, Y. Fish scale-based biochar with defined pore size and ultrahigh specific surface area for highly efficient adsorption of ciprofloxacin. *Chemosphere* **2021**, *287*, No. 131962.
(36) Wang, G.; Yong, X.; Luo, L.; Yan, S.; Wong, J. W. C.; Zhou, J. Structure-performance correlation of high surface area and hierarchical porous biochars as chloramphenicol adsorbents. *Sep. Purif. Technol.* **2022**, *296*, No. 121374.
(37) Song, Q.; Fang, Y.; Wang, J.; et al. Enhanced adsorption of fluoride on Al-modified boron nitride nanosheets from aqueous solution. *J. Alloys Compd.* **2019**, *793*, 512−518.
(38) Li, J.; Lei, N.; Hao, H.; Zhou, J. A series of BCN nanosheets with enhanced photoelectrochemical performances. *Chem. Phys. Lett.* **2017**, *672*, 99−104.
(39) Anna, D.; Michael, K. Exothermic adsorption of chromate by goethite. *Appl. Geochem.* **2020**, *123*, No. 104785.
(40) Khnifira, M.; Boumya, W.; Attarki, J.; Mahsoune, A.; Sadiq, M.; Abdennouri, M.; Kaya, S.; Barka, N. A combined DFT, Monte Carlo, and MD simulations of adsorption study of heavy metals on the

https://doi.org/10.1021/acsomega.3c03348
ACS Omega 2023, 8, 27612−27620

carbon graphite (111) surface. *Chem. Phys. Impact* **2022**, *5*, No. 100121.
(41) Cheng, H.; Huang, Y.; Zhu, Z.; Yu, M.; Xu, W.; Li, Z.; Xiao, Y. Experimental and theoretical studies on the adsorption characteristics of Si/Al-based adsorbents for lead and cadmium in incineration flue gas. *Sci. Total Environ.* **2022**, *858*, No. 159895.
(42) Li, Y.; Su, X.; Gai, A. Preparation of sulfur-doped boron nitride and its adsorption properties on heavy metals in the gas phase. *Environ. Sci. Res.* **2021**, *34*, 2616−2624.
(43) Guo, Z.; Zhang, X.; Kang, Y.; Zhang, J. Biomass-Derived Carbon Sorbents for Cd(II) Removal: Activation and Adsorption Mechanism. *ACS Sustainable Chem. Eng.* **2017**, *5*, 4103−4109.
(44) Wang, L.; Hu, D.; Kong, X.; et al. Anionic polypeptide poly(γ-glutamic acid)-functionalized magnetic Fe_3O_4-GO-(o-MWCNTs) hybrid nanocomposite for high-efficiency removal of Cd(II), Cu(II) and Ni(II) heavy metal ions. *Chem. Eng. J.* **2018**, *346*, 38−49.
(45) Zhang, L.; Chen, Z.; Guo, J.; Xu, Z. Distribution of heavy metals and release mechanism for respirable fine particles incineration ashes from lignite. *Resour., Conserv. Recycl.* **2021**, *166*, No. 105282.
(46) Zhang, X.; Zhang, K.; Lv, W.; Liu, B.; Aikawa, M.; Wang, J. Characteristics and risk assessments of heavy metals in fine and coarse particles in an industrial area of central China. *Ecotoxicol. Environ. Saf.* **2019**, *179*, 1−8.

https://doi.org/10.1021/acsomega.3c03348
ACS Omega 2023, 8, 27612−27620